Spray Coating Experiments: Setups and Methodologies

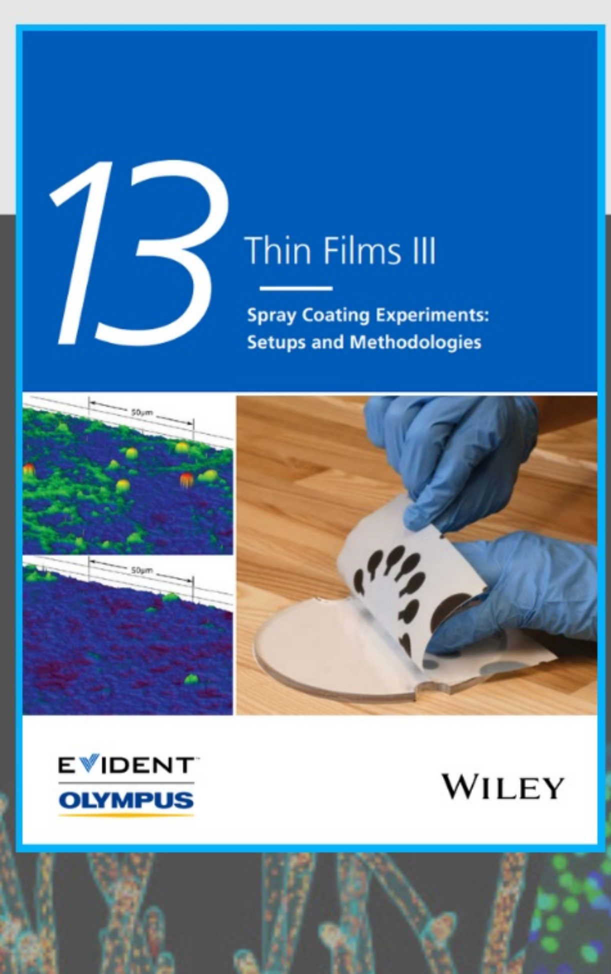

The latest eBook from Advanced Optical Metrology. Download for free.

Spray Coating Experiments: Setups and Methodologies, is the third in our Thin Films eBook series. This publication provides an introduction to spray coating, three article digests from Wiley Online Library and the latest news about Evident's Image of the Year Award 2022.

Wiley in collaboration with Evident, are committed to bridging the gap between fundamental research and industrial applications in the field of optical metrology. We strive to do this by collecting and organizing existing information, making it more accessible and useful for researchers and practitioners alike.

WILEY

Received: 1 December 2022 | Revised: 19 January 2023 | Accepted: 20 January 2023

DOI: 10.1002/ppap.202200229

RESEARCH ARTICLE

PLASMA PROCESSES AND POLYMERS

Low-temperature atmospheric pressure plasma conversion of polydimethylsiloxane and polysilazane precursor layers to oxide thin films

Martin Rudolph[1] | **Peter Birtel**[1] | **Thomas Arnold**[1,2] | **Andrea Prager**[1] | **Sergej Naumov**[1] | **Ulrike Helmstedt**[1] | **André Anders**[1,3] | **Patrick C. With**[1]

[1]Leibniz Institute of Surface Engineering (IOM), Leipzig, Germany

[2]Faculty of Mechanical Science and Engineering, Institute of Manufacturing Science and Engineering, Technische Universität Dresden, Dresden, Germany

[3]Felix-Bloch Institute of Solid State Physics, Leipzig University, Leipzig, Germany

Correspondence

Patrick C. With, Leibniz Institute of Surface Engineering (IOM), Permoser Str. 15, 04318 Leipzig, Germany.
Email: patrick.with@iom-leipzig.de

Funding information

Free State of Saxony and the European Regional Development Fund, Grant/Award Number: 100336119

Abstract

We study the conversion of two polymeric silicon precursor compound layers (perhydropolysilazane and polydimethylsiloxane) on a silicon wafer and polyethylene terephthalate substrates to silicon oxide thin films using a pulsed atmospheric pressure plasma jet. Varying the scan velocity and the number of treatments results in various film compositions, as determined by X-ray photoelectron spectroscopy and Fourier transform infrared spectroscopy. The mechanism suggested for the conversion process includes the decomposition of the precursor triggered by plasma-produced species, the oxidation of the surface, and finally, the diffusion of oxygen into the film, while gases produced during the precursor decomposition diffuse out of the film. The latter process is possibly facilitated by local plasma heating of the surface. The precursor conversion appears to depend sensitively on the balance between the different contributions to the conversion mechanism.

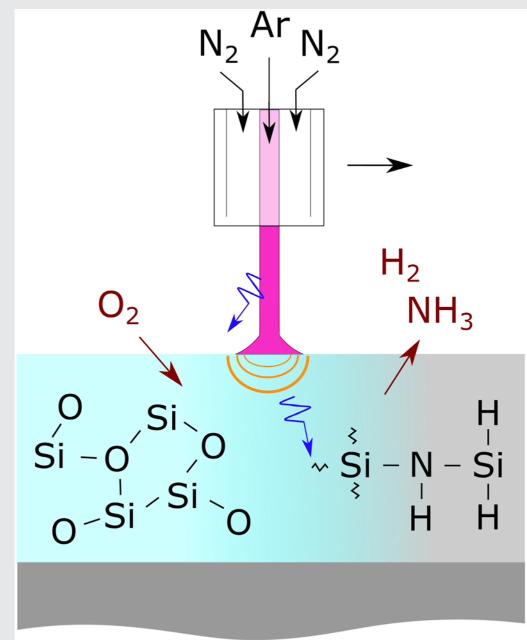

This is an open access article under the terms of the Creative Commons Attribution-NonCommercial-NoDerivs License, which permits use and distribution in any medium, provided the original work is properly cited, the use is non-commercial and no modifications or adaptations are made.
© 2023 The Authors. *Plasma Processes and Polymers* published by Wiley-VCH GmbH.

16128869, 0, Downloaded from https://onlinelibrary.wiley.com/doi/10.1002/ppap.202200229 by Cochrane Germany, Wiley Online Library on [21/03/2023]. See the Terms and Conditions (https://onlinelibrary.wiley.com/terms-and-conditions) on Wiley Online Library for rules of use; OA articles are governed by the applicable Creative Commons License

KEYWORDS
atmospheric pressure plasma, low-temperature conversion, organosilicon precursors, perhydropolysilazane, pulsed discharge

1 | INTRODUCTION

The fabrication of solid thin films by atmospheric pressure plasmas is a cost-effective process. It does not require any vacuum equipment, thus saving investment and running costs. In addition, the compatibility with roll-to-roll machines allows for efficient batch processing.[1] With such a process, flexible substrates like poly (ethylene terephthalate) (PET) foils can be treated. Their temperature sensitivity requires the use of a nonequilibrium or "cold" plasma for the treatment. It is characterized by the temperature of the heavy species (molecules, atoms, ions) being much lower than the electron temperature. A possible application for such a process is the fabrication of flexible protective encapsulation for thin film electronics and (organic) photovoltaic cells, for which a polymer substrate needs to be coated with a permeation barrier layer.[2–4]

Fabrication of inorganic thin films by an atmospheric pressure plasma process can be grouped into deposition and conversion processes. The precursor materials for both processes are typically consisting of a polymeric silicon or metalloidorganic material sometimes mixed with a solvent. For the deposition process, the solution is vaporized using for instance a bubbler with an inert carrier gas (see, e.g., Inomata et al.[5]) or an ultrasonic atomizer (see, e.g., Ward et al.[6]). It then is injected upstream or downstream of a plasma discharge, in which the molecules are ultimately dissociated. The addition of a vaporized precursor is a method compatible with many plasma sources. It works with localized plasma jets and torches[5-7] as well as with large area corona[8] or dielectric barrier discharges (DBDs).[1,9,10] To avoid contact of the plasma with the treated surface, remote plasma reactors are sometimes used.[11,12] A challenge with injecting the precursor into the atmosphere is to avoid particle formation.[1,13-15] These particles are detrimental for many applications, but in particular for gas permeation barriers, where they present diffusion paths through the film.[16] In addition, films prepared by injecting the precursor into the atmosphere often exhibit a porous morphology,[12] which makes this technology not viable for applications in which dense films are required.

In a conversion process, the precursor, usually mixed with a solvent, is transferred in the liquid state directly onto the substrate, where it is treated using an atmospheric pressure plasma. For instance, Tsai et al.[17] spin-coated a solution of liquid nickel acetate mixed with ethanolamine and ethanol onto glass substrates. These were subsequently treated using an atmospheric pressure plasma jet operated in pulsed direct current mode and with N_2 as a working gas. Treatment durations of up to 120 s resulted in solid nickel oxide thin films. The temperature of the gas in the plasma was around 500°C. The temperature of the substrate during processing was not measured.[17]

The fabrication of nanostructures using a similar conversion process termed plasma calcination is proposed by Mudra et al.[18] They prepared composite fibers with a crystalline Al_2O_3 coating and a polymeric core in two steps. First, polymeric fibers were electrospun from a precursor solution made of aluminum nitrate as a metal precursor and polyacrylonitrile in *N*,*N*-dimethylformamide as a base polymer. The original fibers had a diameter of around 1 μm. Plasma treatment resulted in the partial removal of organic contents and lead to a 160 nm-thick crystalline Al_2O_3 film on a polymeric fiber core. The overall fiber still contained 65% of the original polymer. The plasma source employed was a coplanar DBD operated at ambient atmosphere. It was a nonequilibrium atmospheric pressure plasma discharge that could be touched by hand.[19] A similar process using the same plasma source was reported for the production of cerium oxide[20] and titanium oxide[20] fibers. The treatment times were up to 60 min, during which the fiber temperature was not measured. We note here, that the term calcination used to describe the plasma-assisted conversion is misleading as calcination per definition is a high-temperature process.[21] Indeed, the term *conversion* seems to be more appropriate.

While the conversion of an organic precursor layer to a thin film via an atmospheric pressure plasma process is widely applied, the mechanisms leading to thin film conversion remain rather fuzzy. Here, we discuss the conversion of perhydropolysilazane (PHPS) and polydimethylsiloxane (PDMS) coated onto a substrate, using a pulsed atmospheric pressure plasma jet (pAPPJ). We present the general experimental setup in Section 2. The analysis of the plasma-treated thin films using attenuated total reflectance Fourier transform infrared spectroscopy (ATR-FTIR), X-ray photoelectron spectroscopy (XPS), and scanning electron microscopy (SEM) are presented in Section 3. Based on these results, we discuss a possible mechanism relevant to converting polymeric silicon precursor layers at low temperatures into oxide thin films in Section 4, before we summarize the work in Section 5.

16128869, 0, Downloaded from https://onlinelibrary.wiley.com/doi/10.1002/ppap.202200229 by Cochrane Germany, Wiley Online Library on [21/03/2023]. See the Terms and Conditions (https://onlinelibrary.wiley.com/terms-and-conditions) on Wiley Online Library for rules of use; OA articles are governed by the applicable Creative Commons License

2 | EXPERIMENTAL SETUP

The atmospheric pressure plasma is produced by a custom-built plasma jet source excited by a pulsed microwave at 2.45 GHz. The pAPPJ originates from an inner tube in which a flowing Ar gas is excited. An outer tube serves to shield the jet from the atmosphere with a flow of N_2. The Ar and N_2 flows were 400 and 300 sccm, respectively (Figure 1). The shielding gas, however, does not completely prevent the entrainment of the surrounding air. Therefore, successive radial diffusion of oxygen into the center of the plasma jet is observed, and reactive oxygen/nitrogen species are formed in the discharge. The pulse duration was 10 µs, and the delay (off-time) was adjusted for an effective input power into the plasma jet of approximately 3 W of average dissipated power. The distance between the outlet of the plasma jet and the sample surface was $h = 6$ mm. For the process, we had the plasma jet meander over the sample surface as depicted in Figure 1. The distance between the two lines was $\Delta z = 0.5$ mm with an estimated line width of 2 mm. For the samples, we varied the scan velocity between $v_{scan} = 2$ and 16 mm/s and the number of treatments between 1 and 10 times.

Two Si-containing precursors were selected for their different stability to oxidation (Figure 2). These were ultraviolet (UV)-curable PDMS (micro resist technology GmbH) and prehydrolyzed PHPS (Merck Performance Materials). Latter bears a significantly higher pot time under ambient conditions compared to pure PHPS. Both, the PDMS and PHPS precursor were dissolved in *n*-dibutyl ether (>99%; Merck). For each sample, the corresponding precursor was spin-coated onto small-area Si wafer (1 cm × 1 cm) and large-area (ca. 5 cm × 5 cm) PET foil substrates (Melinex 506; $d_{PET} = 100$ µm) and dried at 50°C under nitrogen atmosphere.

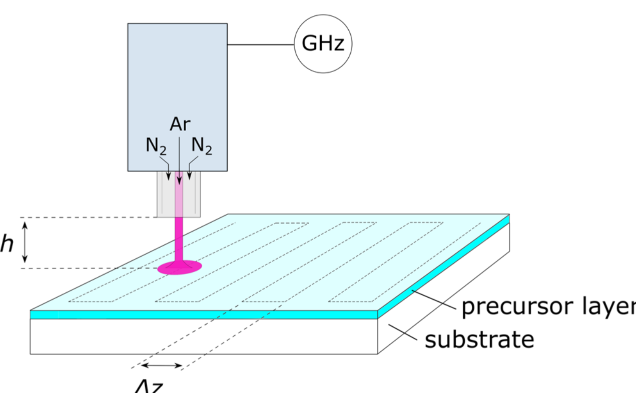

FIGURE 1 Schematic of the experimental setup for scanning/treatment of a sample surface using a custom-built pulsed atmospheric pressure plasma jet.

The plasma-treated samples on Si and PET were both analyzed by ATR-FTIR with a Varian 670 spectrometer (Agilent Technologies, Inc.) equipped with a variable grazing angle ATR unit (VariGATR, Harrick, Ge ATR crystal, at 65°). Spectra were recorded for 1 cm × 1 cm large samples between 4000 and 600 cm^{-1} with a resolution of 1 cm^{-1} using an MCT detector. The spectra shown in this manuscript are not background subtracted. We used this technique to analyze the decomposition of the films via the decrease of N–H and Si–H peak areas between, before, and after the plasma treatment. At the same time, the technique revealed the oxidation of the precursor film via an increase in the peak area of the Si–O stretching vibration in the ATR-FTIR spectrum. Each experiment was repeated two to five times. Each of these samples was measured by ATR-FTIR. The data points in the plots below, therefore, show the average value while the uncertainty bars indicate the standard deviation. FTIR-related symbols ν, δ, ρ, and ω denote stretching, bending, rocking, and wagging modes, respectively. The indices 'as' and 's' denote asymmetric and symmetric vibrations, respectively.

The chemical composition of converted films was studied by XPS with an AXIS Ultra (KRATOS Analytical Ltd) using a monochromatized Al K_α X-ray excitation source (150 W, 15 kV/10 mA, spot size 700 µm × 300 µm). Depth profiles were obtained by alternating steps of film sputtering with argon ions (0.2 kV, sputter area 2 mm × 2 mm) and XPS analysis (10/30 s per step). The samples were not baked before the XPS measurement to not change the chemical composition after the low-temperature plasma treatment. The first data point measured on the surface of the thin film may therefore deviate from the trend just below the surface. The average thin film composition was calculated based on the depth profile data of the thin film excluding the interface regions.

The thin film morphology was investigated by SEM on an ULTRA 55 system (Carl Zeiss SMT) at an

(a) PHPS
(b) PDMS

FIGURE 2 Simplified structure diagrams of (a) the perhydropolysilazane (PHPS) and (b) the polydimethylsiloxane (PDMS) precursor used in this study.

16128869, 0, Downloaded from https://onlinelibrary.wiley.com/doi/10.1002/ppap.202200229 by Cochrane Germany, Wiley Online Library on [21/03/2023]. See the Terms and Conditions (https://onlinelibrary.wiley.com/terms-and-conditions) on Wiley Online Library for rules of use; OA articles are governed by the applicable Creative Commons License

acceleration voltage of 1 kV. Thin film thicknesses were determined by spectral reflectance measurements (F20 instrument; Filmetrics).

Density functional theory (DFT) calculations were carried out using the Minnesota functional family (M06), which is parameterized for organometallic and noncovalent interactions,[22] as also shown in previous works on metalorganic complexes.[23–25] The molecular geometries and energies of the considered molecules were calculated at the M06/LACVP** level of theory as implemented in Jaguar 9.6 program suite.[26] The LACVP** basis set uses the standard 6-31G(d,p) basis set for light elements and the LAC pseudo potential for heavier elements.[27] Frequency calculations were done in harmonic approximation, at the same level of theory to characterize the stationary points on the potential surface, to analyze the frequency spectra at the standard temperature of 298.15 K using unscaled vibrations, which can result in slightly overestimated frequency positions.

3 | RESULTS

3.1 | Comparison between PHPS and PDMS precursor layers

We start by comparing the conversion of a PHPS and a PDMS precursor, coated on a monocrystalline Si wafer substrate, using a pAPPJ. The layers had initial film thicknesses of 110 ± 5 nm for PDMS and 131 ± 3 nm for PHPS, respectively. They were treated using the pAPPJ with the gas flow rates and electrical discharge settings described above. For that, the plasma jet was scanned over the surface of the precursor layer with a velocity of 2 mm/s at 3 W of average dissipated power (Figure 1) and a distance of $\Delta z = 0.5$ mm between two line scans. Each sample in this section was treated once.

Figure 3 shows the ATR-FTIR spectrum of an untreated PHPS precursor film with its characteristic vibration bands for N–H (ν(N–H) 3374 cm^{-1}, δ(N–H) 1180 cm^{-1}), Si–H (ν(Si–H) 2163 cm^{-1}, δ(Si–H) 1003 cm^{-1}, ω(Si–H) 829 cm^{-1}), Si–N (ν(Si–N) 922 cm^{-1} and 880 cm^{-1}), as well as Si–O (ν(Si–O) 1083 cm^{-1}). After a pAPPJ treatment with a scanning speed of 2 mm/s, the intensity of the ν(Si–H) band decreases. Based on the ν(Si–H) peak area before and after plasma treatment, a decrease of ν(Si–H) peak area of $61.4 \pm 5.9\%$ is calculated. At the same time, the peak area of the Si–O band increases significantly indicating the oxidation of the precursor film.

Upon oxidation, a blue shift of the ν(Si–H) band to higher wavenumbers (2163–2172 cm^{-1}, $\Delta = 9$ cm^{-1}) is observed, which can be explained by substituting oxygen for nitrogen in the polymeric structure. This hypothesis is supported by DFT-calculated vibrational spectra of simplified eight-ring structures with and without partial substitution of oxygen for nitrogen (Figure 3). To exclude the influence of a hydrolysis reaction, reference

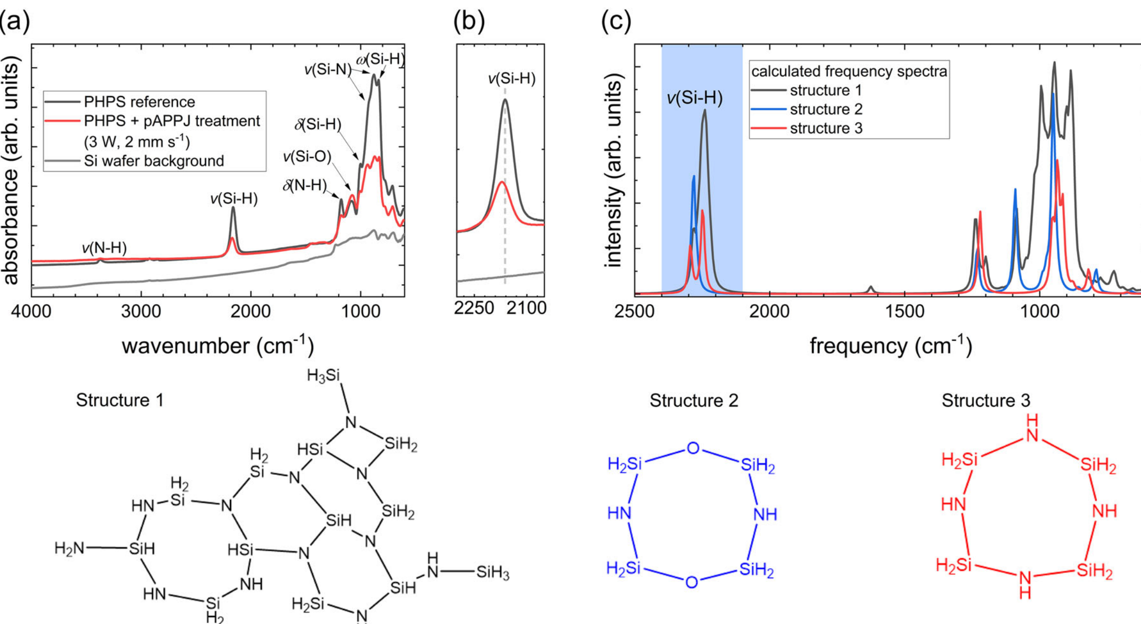

FIGURE 3 Attenuated total reflectance Fourier transform infrared spectroscopy spectra of PHPS precursor films on Si-wafer substrates before and after plasma treatment: (a) assignment of the characteristic vibration bands; (b) magnification of the ν(Si–H) region; (c) calculated PHPS spectrum for a complex ring structure as well as for simplified eight-ring structures with and without substitution of oxygen for nitrogen (corresponding structures are shown below the spectra).

16128869, 0, Downloaded from https://onlinelibrary.wiley.com/doi/10.1002/ppap.202200229 by Cochrane Germany, Wiley Online Library on [21/03/2023]. See the Terms and Conditions (https://onlinelibrary.wiley.com/terms-and-conditions) on Wiley Online Library for rules of use; OA articles are governed by the applicable Creative Commons License

16128869, 0, Downloaded from https://onlinelibrary.wiley.com/doi/10.1002/ppap.202200229 by Cochrane Germany, Wiley Online Library on [21/03/2023]. See the Terms and Conditions (https://onlinelibrary.wiley.com/terms-and-conditions) on Wiley Online Library for rules of use; OA articles are governed by the applicable Creative Commons License

precursor layers were stored under atmospheric conditions for times comparable to the plasma treatment and subsequent analysis. The resulting ATR-FTIR spectra show no significant differences, for example, for ν(Si–H), δ(N–H), and ν(Si–O) compared to freshly prepared precursor layers (see Figure S1). We therefore attribute the observed oxidation solely to the plasma treatment of the sample. As a result of the pAPPJ treatment, the film thickness slightly decreased from 131 ± 3 nm for the untreated precursor to 112 ± 2 nm for the converted thin film.

Similar film densification has been observed for vacuum UV (VUV) light-induced conversion of PHPS described by Prager et al.[28] In their work, the conversion was described as a two-step process. The first step comprised precursor excitation and initial decomposition with simultaneous formation of H_2 and NH_3.[28] Formed radical species in the precursor layer reacted with O_2 in a second step to form silicon oxide. It could be shown that the mass transfer of the formed gas molecules out of the film, and of oxygen into it, played an essential role in the conversion process and its overall kinetics. We suggest that similar processes are relevant for the conversion attempted here using a pAPPJ.

In contrast to PHPS, PDMS is characterized by its stability under atmospheric conditions and against reactions with oxygen and water vapor. Moreover, the precursor itself already contains oxygen (Figure 2b). For a complete conversion toward SiO_2, methyl groups have to be removed and replaced by oxygen. Figure 4 shows the ATR-FTIR spectra of the PDMS precursor layer on Si substrate exhibiting the characteristic bands for CH_3 ($\nu_{as}(CH_3)$ 2963 cm^{-1}, $\nu_s(CH_3)$ 2904 cm^{-1}, $\delta(CH_3)$ 1260 cm^{-1}, and $\rho(CH_3)$ 780 cm^{-1}) and Si–O (ν_{as}(Si–O) 1082 cm^{-1} and ν_s(Si–O) 1019 cm^{-1}).[29] After pAPPJ treatment with a scan speed of 2 mm/s, methyl-related peak intensities decrease compared to those for Si–O. This can be attributed to the removal of the methyl groups from the precursor layer, as was also described by Berchidevsky et al.[29] for the UV ozone oxidation of PDMS films. Based on the methyl-related peak areas for $\delta(CH_3)$, $\nu_{as}(CH_3)$, and $\nu_s(CH_3)$, a decrease of peak areas by 18 ± 2% is determined. Upon pAPPJ treatment, a slight blue shift of the methyl-based vibrations by 0.5–0.8 cm^{-1} is observed, also indicative of oxidation of the film.

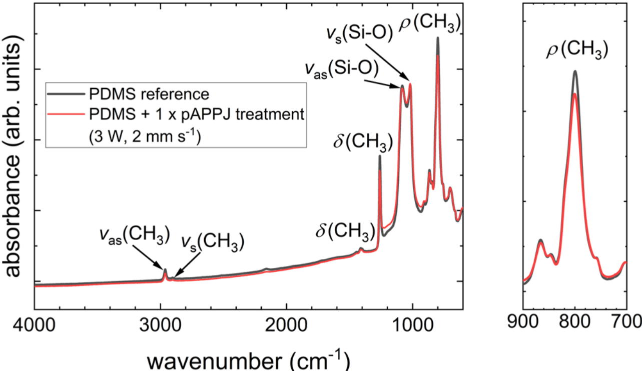

FIGURE 4 Attenuated total reflectance Fourier transform infrared spectroscopy (ATR-FTIR) spectra of polydimethylsiloxane (PDMS) precursor films onto Si-wafer substrates before and after plasma treatment and assignment of the characteristic vibration bands (left) as well as a magnification of the $\rho(CH_3)$ peak (right). pAPPJ, pulsed atmospheric pressure plasma jet.

The thin films obtained after the pAPPJ treatment show oxidic Si^{4+} (103.5 eV) for both, the PHPS and the PDMS samples (see Figure S2). XPS depth profiles show the oxygen distribution in the thin films. The thin film from the PHPS precursor (Figure 5a) has a peak in oxygen content close to the surface (52 at%), from where the oxygen content is slowly decreasing toward the interface with the silicon wafer (45 at%). This variation of oxygen content as a function of film depth could be explained by the abundant supply of oxygen from the surrounding air to the surface of the film. At the same time, the diffusion of oxygen in the film is slow, which delays the arrival of oxygen species deep in the film. The oxygen diffusion in the film is therefore likely the rate-limiting step of the conversion.

For the PDMS sample, film oxidation is limited to the near-surface region (Figure 5b), with an oxygen content decreasing from 55 at% down to approximately 30 at% (corresponding to the composition of the untreated precursor film). In addition, we observe a distinctive decrease in carbon content at the surface of the film down to 17 at%, while the carbon content deeper in the film is 37 at%. A possible reason for the limitation of the conversion to the near-surface region could be film densification. As the film decomposes and hydrogen and nitrogen-containing species are released through the surface of the film, the film densifies, hampering further diffusion of gaseous species out of the film and of oxygen into the film.

3.2 | Velocity-dependence for PHPS samples

The previous section indicates a faster conversion of the PHPS compared to the PDMS precursor by the pAPPJ. In the following, we therefore focus on the investigation of the pAPPJ-induced conversion of PHPS.

To study the conversion kinetics, we varied the velocity of the pAPPJ from $\nu_{scan} = 2$ mm/s (as used in the previous sections) to 16 mm/s, thus, decreasing the

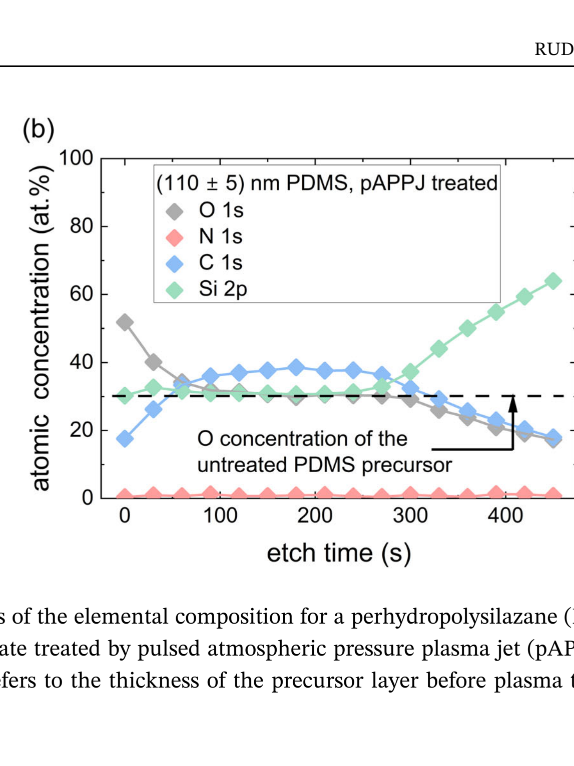

FIGURE 5 X-ray photoelectron spectroscopy (XPS) depth profiles of the elemental composition for a perhydropolysilazane (PHPS)- (a) and a polydimethylsiloxane (PDMS)-precursor (b) film on a Si substrate treated by pulsed atmospheric pressure plasma jet (pAPPJ) with a velocity of $v_{scan} = 2$ mm/s from XPS measurements. The thickness refers to the thickness of the precursor layer before plasma treatment.

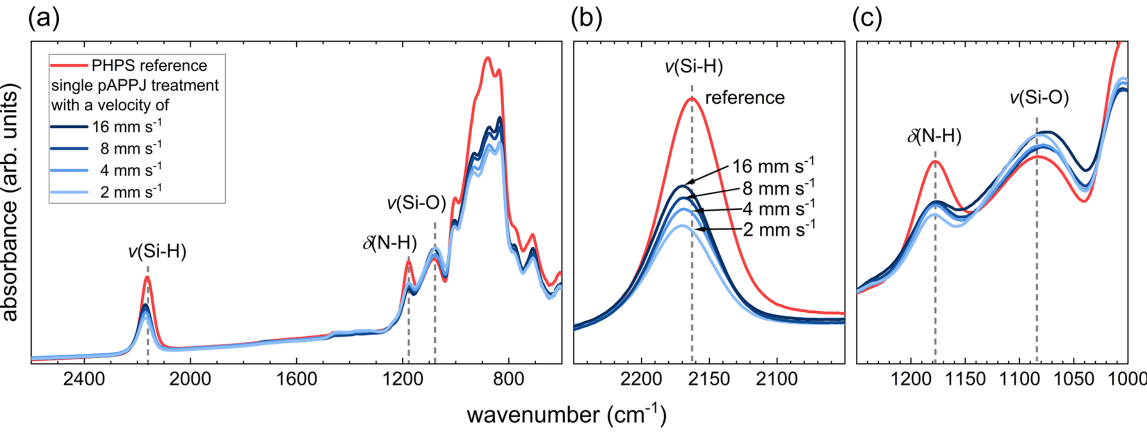

FIGURE 6 Attenuated total reflectance Fourier transform infrared spectroscopy spectra of a perhydropolysilazane (PHPS)-coated Si substrate with a thickness of approximately 131 ± 3 nm treated with the pulsed atmospheric pressure plasma jet (pAPPJ) once with scan velocities between 2 and 16 mm/s. (a) shows an overview spectrum, (b) and (c) show a magnification of the ν(Si–H), δ(N–H), and ν(Si–O) peaks, respectively.

effective residence time of the plasma jet on a given spot on the sample. An average dissipated RF power of 3 W was used for all experiments described below. Panel (a) of Figure 6 shows an overview spectrum while a detailed view of the ν(Si–H) and δ(N–H) peaks is shown in Panels (b) and (c), respectively. The plasma-treated samples show considerably smaller peak areas for the δ(N–H) and ν(Si–H) peaks compared to that of the initial PHPS precursor. Differences in treatment velocity on the decomposition of the precursor, however, remain small.

Figure 7 shows the normalized peak areas determined from the ATR-FTIR spectra. Halving the velocity v_{scan} doubles the effective residence time of the plasma jet at one spot. As a consequence, the ν(Si–H) peak area decreases when lowering the scan velocity of the pAPPJ. However, it can be seen that the percental decrease of the ν(Si–H) peak area does not decrease by a factor of 2 when the velocity is decreased by a factor of 2 (0.56 vs. 0.43 at 4 and 2 mm/s, respectively). The δ(N–H) peak area decreases at a higher rate compared to the ν(Si–H) peak area at all treatment velocities investigated here. The ν(Si–O) peak area is indicative of the oxidation of the film. Here, we observe the ν(Si–O) peak area to increase with increasing velocity v_{scan}. This is despite the fact that a higher scan velocity means a shorter residence time of the pAPPJ at one spot. We attempt an explanation of this in Section 3.4.

SEM images of the PHPS precursor samples after the pAPPJ treatment with a velocity of $v_{scan} = 2$ mm/s show surface structures with dimensions of 80–280 nm

16128869, 0, Downloaded from https://onlinelibrary.wiley.com/doi/10.1002/ppap.202200229 by Cochrane Germany, Wiley Online Library on [21/03/2023]. See the Terms and Conditions (https://onlinelibrary.wiley.com/terms-and-conditions) on Wiley Online Library for rules of use; OA articles are governed by the applicable Creative Commons License

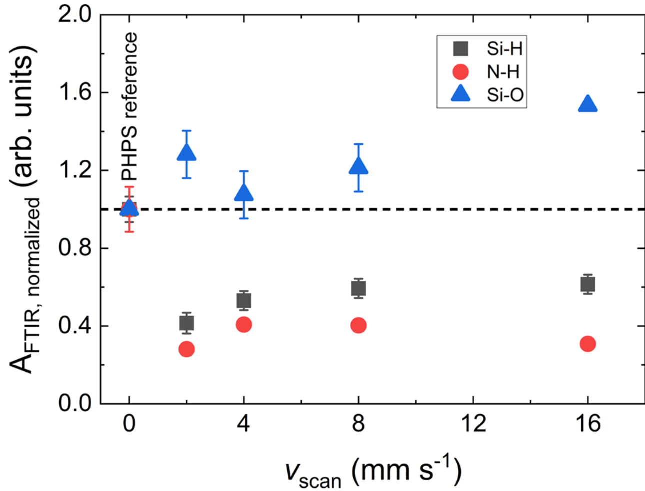

FIGURE 7 Normalized peak areas of δ(N–H), ν(Si–H), and ν (Si–O) extracted from the attenuated total reflectance Fourier transform infrared spectroscopy spectra shown in Figure 6.

(Figure 8b). A view of the cross-section image suggests that these structures are craters with depths of about 20 nm (Figure 8c). Increasing the velocity to 16 mm/s and, thus reducing the effective residence time with the pAPPJ, has no visible effect on the crater size and morphology (Figure 8d–f). A possible explanation for these craters could be an initial fast decomposition reaction of the PHPS precursor with the formation of gaseous reaction products such as H_2 and NH_3 in contact with the plasma jet, which could lead to the formation and accumulation of gas inside the thin film. Upon placing these samples in the vacuum of the microscope, these gas bubbles burst and leave behind the craters observed. In addition, for the less reactive PDMS precursor layers, no craters appeared after the pAPPJ treatment (see Figure S3). Effects from substrate charging on the surface morphology cannot be excluded but are considered unlikely because the plasma jet provides a high flux of species of either polarity, that would immediately neutralize any surface charge.

3.3 | Thickness effects

The PHPS samples from Section 3.1 show a decreasing oxygen concentration with film depth, which implies that the oxidation of the precursor is diffusion-limited (Figure 5a). Here, we therefore study the film conversion for a 131 ± 3 nm thick PHPS film as well as for a 40 ± 4 nm thick PHPS film. Both films were treated using the flow rates of Ar and N_2 described above and a scan velocity of 2 mm/s.

Figure 9 shows the XPS depth profiles of the elemental composition for the two films with striking differences. The C and N concentrations of the 40 nm-thick film are significantly lower compared to the C and N concentrations of the 131 nm-thick film. This indicates a more complete decomposition and release of the gaseous species from the thinner films compared to the first 40 nm of the thick film. Moreover, the oxygen content is considerably higher in the thin sample compared to the thick sample. While the concentration is on average 50 at% in the surface region of the 131 nm-thick films, it is approximately 60 at% for the 40 nm-thick film, approaching SiO_2 stoichiometry. In comparison, a thermal conversion at 600°C and photochemical conversion at room temperature resulted in an oxygen-deficient stoichiometry of $SiO_{1.48}N_{0.01}$ and $SiO_{1.84}N_{0.03}$, respectively (determined by XPS).[30]

The reason for the faster precursor decomposition can be directly related to the thinner film, which implies shorter average diffusion lengths for C- and N-containing species from their origin to the film surface where the gaseous products are released. The higher oxygen concentration in the first 40 nm under the surface of the two films is likely due to the lower diffusivity of oxygen in the dense Si wafer compared to the diffusivity in the less dense precursor film. Oxygen incorporated into the thin film is therefore accommodated in a smaller available volume which shows up as a higher oxygen concentration. This result suggests that there is potential for increasing the oxygen content also in the 131 nm-thick films toward an ideal SiO_2 stoichiometry by further optimizing the process.

3.4 | Influence of the number of treatment steps

In Section 3.2 we have observed that lowering the effective residence time of the pAPPJ at one spot by increasing the velocity v_{scan}, increases the overall oxygen concentration in the film. Here, we increase the effective residence time by keeping the scan velocity constant and increasing the number of treatment steps. The number of treatment steps is the number of consecutive single treatments of the pAPPJ of the sample where every single treatment is done with the scan velocity of v_{scan} = 2 mm/s at an average dissipated RF power of 3 W.

Figure 10 shows the XPS depth profiles of the elemental composition of two thin films treated once and 10 times, respectively. While the Si content as well as the N and C content vary slightly between the samples, the most striking difference is a considerable difference in oxygen concentration. For both samples, the oxygen concentration decreases with increasing depth of the film, but the difference is approximately 10 percentage

16128869, 0, Downloaded from https://onlinelibrary.wiley.com/doi/10.1002/ppap.202200229 by Cochrane Germany, Wiley Online Library on [21/03/2023]. See the Terms and Conditions (https://onlinelibrary.wiley.com/terms-and-conditions) on Wiley Online Library for rules of use; OA articles are governed by the applicable Creative Commons License

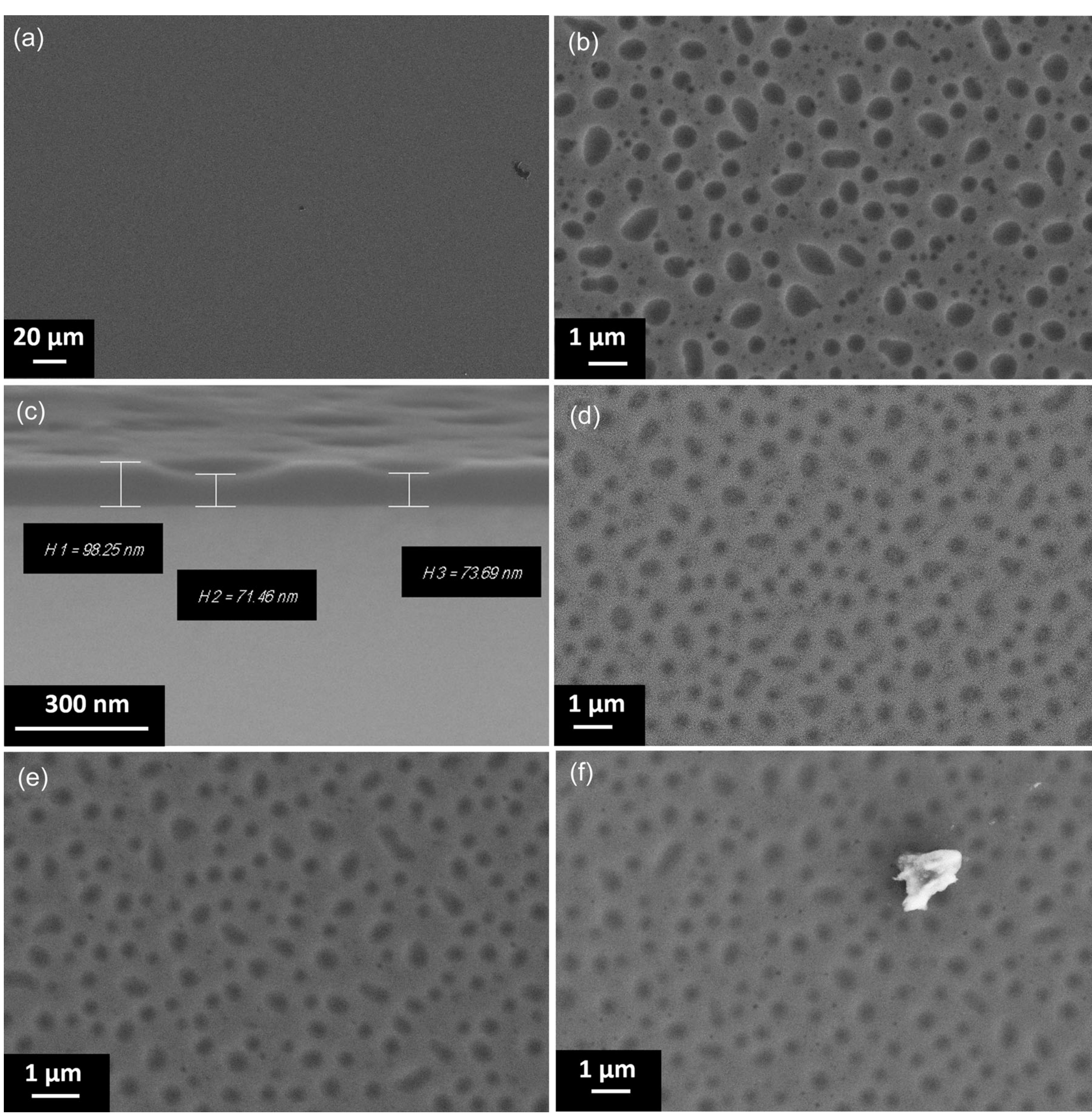

FIGURE 8 Scanning electron microscopy images of the thin film morphology of a perhydropolysilazane precursor layer after pulsed atmospheric pressure plasma jet treatment. (a, b) Samples treated at a scan velocity of 2 mm/s at different magnifications, (c) a cross-section, (d–f) samples treated at scan velocities of 4, 8, and 16 mm/s, respectively.

points close to the surface and slightly less when going toward the interface with the Si wafer.

Figure 11 shows the elemental composition of films depending on the number of treatment steps. The composition is averaged over the film depth where we have excluded the surface and the interface of the films with the substrate. The graph shows how the N and C concentrations decrease with consecutive treatments, while the oxygen concentration increases. After 10 treatments the composition of the thin film is $SiO_{1.43}N_{0.08}C_{0.06}$.

At first glance, these results appear to contradict the observations from Section 3.2 where decreasing the scan velocity, or increasing the residence time of the pAPPJ on one spot, leads to a lower oxygen content in the film. Here, increasing the effective residence time of the pAPPJ on one spot by increasing the number of consecutive treatments, increases the oxygen content in the film. The seeming contradiction could be explained by the film densification mechanism already mentioned in Section 3.1. When decreasing the scan velocity, the conversion rate likely increases as the intensity of plasma-produced species (VUV photons and oxygen radicals) is higher. This could, following up the discussion in Section 3.1, lead to film densification at the surface, hampering further diffusion of gaseous byproducts out of the film and of oxygen into the film. In contrast, when increasing the number of treatment steps, the diffusion processes can take place during the

16128869, 0, Downloaded from https://onlinelibrary.wiley.com/doi/10.1002/ppap.202200229 by Cochrane Germany, Wiley Online Library on [21/03/2023]. See the Terms and Conditions (https://onlinelibrary.wiley.com/terms-and-conditions) on Wiley Online Library for rules of use; OA articles are governed by the applicable Creative Commons License

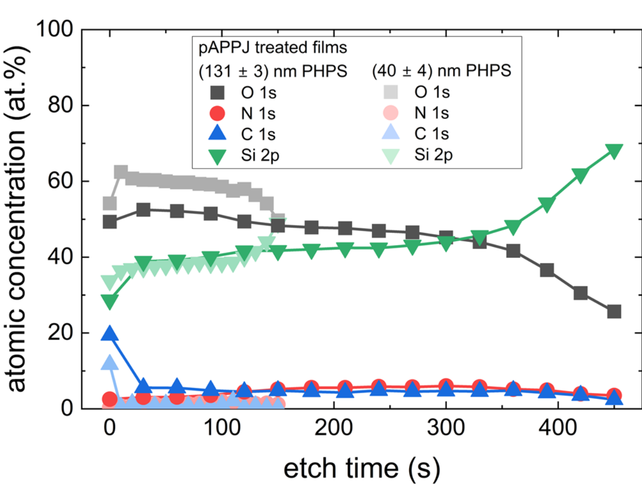

FIGURE 9 X-ray photoelectron spectroscopy (XPS) depth profiles of the elemental composition from XPS measurements for two perhydropolysilazane (PHPS) samples with thicknesses of 131 ± 3 and 40 ± 4 nm, respectively. Both films are treated one single time at a scan velocity of 2 mm/s.

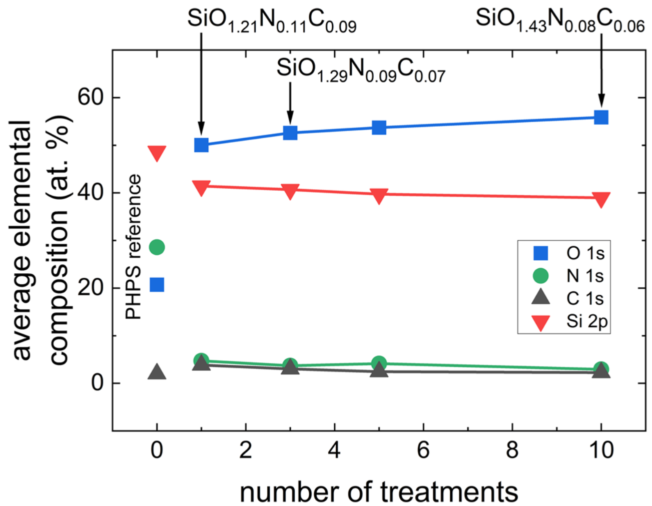

FIGURE 11 Elemental composition from X-ray photoelectron spectroscopy analysis of the perhydropolysilazane (PHPS) films as a function of the number of treatment steps averaged over the film thickness, excluding the surface of the film as well as the interface.

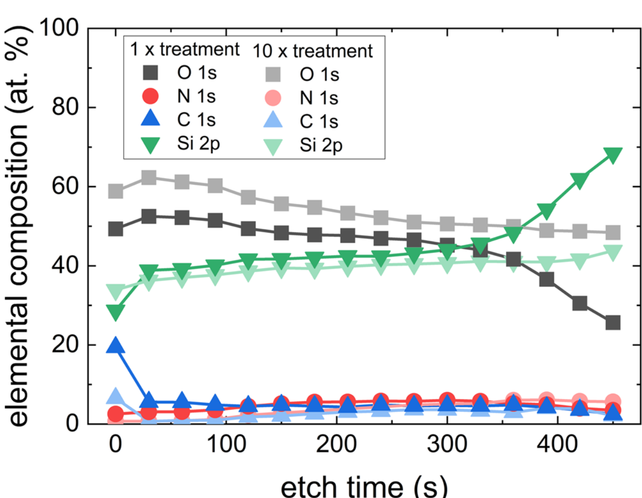

FIGURE 10 X-ray photoelectron spectroscopy depth profiles of the elemental composition of the perhydropolysilazane film on a Si substrate after a single treatment step and 10 consecutive treatment steps.

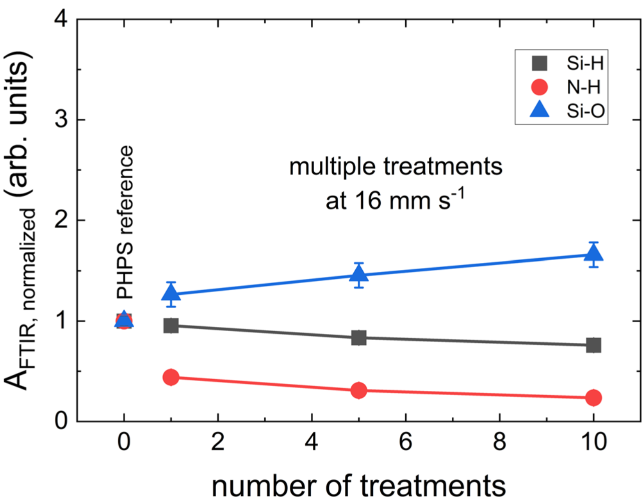

FIGURE 12 Normalized peak areas of ν(Si–H), δ(N–H), and ν(Si–O) extracted from the attenuated total reflectance Fourier transform infrared spectroscopy data of the experiment with a scan velocity of v_{scan} = 16 mm/s and a different number of treatments steps.

individual treatment steps, which may promote the conversion also deep in the precursor layer. For process developments, it, therefore, appears to be important to keep a fine balance between the decomposition and oxidation steps on one side and the diffusion processes on the other.

3.5 | PHPS conversion on PET substrates

In the Introduction, we mention the possibility of treating temperature-sensitive substrates when using a nonequilibrium or cold plasma. To prove the compatibility of temperature-sensitive substrates with a pAAPJ, we deposited a 131 ± 3 nm-thick layer of PHPS onto a temperature-sensitive PET film and subsequently treated it with the pAPPJ.

The conversion of the PHPS precursor films on PET substrates is deduced from ATR-FTIR measurements shown in Figure 12. The samples are treated using a scan velocity of v_{scan} = 16 mm/s and treated once, 5 or 10 times. The evaluation of the ATR-FTIR spectra shows increasing degrees of conversion with increasing numbers of treatment

16128869, 0, Downloaded from https://onlinelibrary.wiley.com/doi/10.1002/ppap.202200229 by Cochrane Germany, Wiley Online Library on [21/03/2023]. See the Terms and Conditions (https://onlinelibrary.wiley.com/terms-and-conditions) on Wiley Online Library for rules of use; OA articles are governed by the applicable Creative Commons License

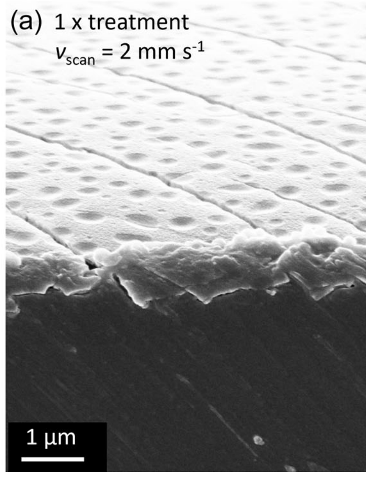

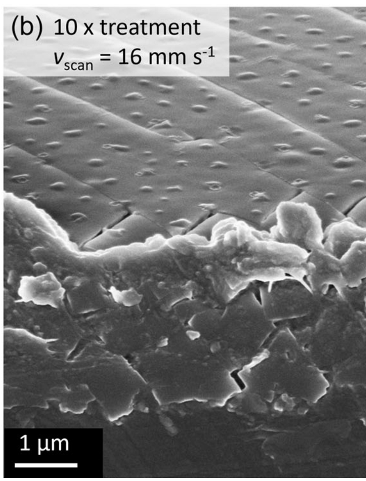

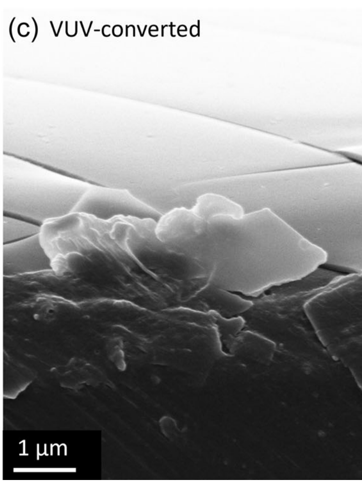

FIGURE 13 Scanning electron microscopy images of a plasma-treated perhydropolysilazane film on a polyethylene terephthalate substrate with (a) one treatment at $v_{scan} = 2$ mm/s ($t_{res} = 1.0$ s) and (b) 10 treatments at 16 mm/s ($t_{res} = 1.25$ s). Panel (c) shows a vacuum ultraviolet (VUV)-converted film for comparison. Details of its preparation can be found in Prager et al.[28] The cracks in the thin film observed on all samples, going from the upper left corner to the lower right corner, are an artifact of the sample preparation.

steps, as reflected by decreasing values for ν(Si–H) bands and increasing values for ν(Si–O) bands, respectively, in line with the results of Section 3.5.

Figure 13 shows SEM images of a single time plasma-treated sample at a velocity of $v_{scan} = 2$ mm/s (Figure 13a) and a plasma-treated sample that is treated 10 times at a scan velocity of 16 mm/s (Figure 13b). For both samples, the effective residence times of the pAPPJ on one spot are very similar. However, the SEM images show very different surface morphologies. The sample treated at a slow scan velocity shows craters, while the sample treated multiple times using a high scan velocity shows a protruding structure. This suggests that the pattern forming on the surface of the plasma-treated samples is strongly dependent on the kinetics of the conversion. For comparison, Figure 13c shows the smooth surface of a VUV-converted thin film.[28]

After the plasma treatment, no visible damage is observed on the PET foils, which suggests that the plasma conditions applied in this study have a negligible thermal impact on the substrates. Labeling the process as "low-temperature" is therefore justified by the ability to fabricate a silicon oxide thin film on a temperature-sensitive substrate such as PET.

4 | DISCUSSION

Above, we present experiments with the goal of converting PDMS and PHPS precursor layers to a silicon oxide thin film using a pAPPJ under different conditions. The results indicate a wide range of parameters for exploring new process windows. In the following, we discuss possible contributions to the conversion process, which will help to design new experiments.

At first glance, the here-discussed plasma conversion process resembles that of a VUV conversion of organometallic layers to oxide thin films. Prager et al.[28] describe a VUV process with a PHPS precursor converted to a silicon oxide thin film. They used a Xe_2* lamp (among others) with an excimer continuum around 172 nm. In this process, the VUV photons decompose an organic precursor layer by cleaving bonds homolytically. This forms a layer containing silicon radicals as well as H_2 and NH_3 gas. While the latter can diffuse out of the film, the silicon radicals at the surface of the layer form oxides using oxygen from the surrounding atmosphere. A diffusion process ensures the complete oxidation of the thin film.

C-conversion process (Figure 14). Plasma-produced species, like VUV radiation can penetrate into the precursor layer to form Si radicals by cleaving bonds. VUV radiation is, for example, emitted by argon plasma that includes the excimer continuum at 126 nm.[31] As a result, gaseous species accumulate in the film. Oxygen from the surrounding air, ozone, or oxygen radicals produced in the plasma source can then react with the Si radicals at the surface. A diffusion process transports oxygen into the film. The diffusion process may be promoted by local heating from the plasma source. This could be induced by the quenching of excited species at the surface of the precursor layer, from the release of reaction enthalpy during oxidation, or from the absorption of radiation. This local heating is mostly limited to the surface of the

16128869, 0, Downloaded from https://onlinelibrary.wiley.com/doi/10.1002/ppap.202200229 by Cochrane Germany, Wiley Online Library on [21/03/2023]. See the Terms and Conditions (https://onlinelibrary.wiley.com/terms-and-conditions) on Wiley Online Library for rules of use; OA articles are governed by the applicable Creative Commons License

(a) fragmentation of precursor by photons

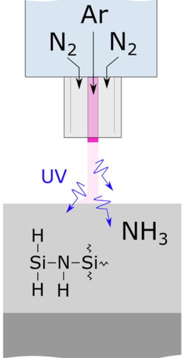

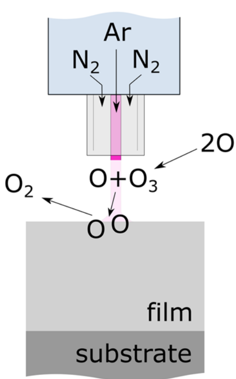

(c) oxygen and gas diffusion from local heating

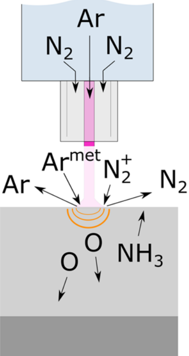

FIGURE 14 Suggested contributions to the conversion of the perhydropolysilazane (PHPS) precursor layer using an atmospheric pressure plasma jet. (a) The fragmentation of the precursor via energetic (vacuum ultraviolet) photons. (b) The production of ozone or oxygen radicals from O_2 in the atmosphere that can react with the surface of the PHPS film. (c) The diffusion of these oxygen species into the precursor layer, consecutively oxidizing it. This step could be promoted by local heating of the surface by the plasma source. (c) Likely to be rate-limiting. Note that the selection of chemical species in the schematic is for illustrative purposes only and should not be understood as a comprehensive list of species.

precursor layer and remains below the threshold for damaging the temperature-sensitive PET substrate (Section 3.5).

For PHPS and PDMS we observe strikingly different conversion results, though. The reason for the PDMS conversion to be limited to the near-surface region compared to PHPS could be a faster decomposition of the precursor followed by the release of gaseous species and the oxidation of the film. If these steps proceed faster than the diffusion of oxygen species deep into the film, then the film densifies at the surface, effectively limiting further diffusion of species out of the film and deep into the film. A possible gaseous by-product from the decomposition of PDMS is CH_4. This has a much larger kinetic diameter (380 pm[32]) compared to ammonia (260 pm[33]), a by-product of PHPS, which additionally could hamper the conversion process of PDMS compared to PHPS.

A purely VUV-driven and a plasma conversion process, therefore, differ in three aspects. The source of VUV photons using a plasma process is right at the surface of the precursor layer. This allows us to run the process in ambient air, which is known to absorb a large part of the VUV spectrum. Second, the plasma produces oxygen radicals such as ozone or atomic oxygen, possibly accelerating surface oxidation. Finally, the plasma may heat the surface of the thin film to promote the diffusion of oxygen species into the film as well as the release of gases formed inside the film.

5 | SUMMARY

We here discuss a method to convert wet-chemically-coated polymeric silicon compound (precursor) layers into solid thin films using a pAPPJ. In such a process, PHPS precursor layers are partially converted into a SiO_x thin film. We suggest three contributions that are relevant to the overall conversion process: First, plasma-produced species, such as VUV photons, decompose the precursor by cleaving bonds to hydrogen and nitrogen. Second, plasma-produced oxygen radicals and ozone bond to the surface of the film. Third, gaseous species produced during the plasma-induced precursor decomposition diffuse out of the film. At the same time, oxygen diffuses from the surface into the film. The diffusion of species into and out of the film appears to be hampered if the decomposition and oxidation proceed too fast. We explain this by densification of the thin film surface which hampers further diffusion of species in the film. This indicates that for an effective conversion process, one needs to find a balance between the decomposition and oxidation kinetics on one side and diffusion kinetics on the other. We show that the conversion process is compatible with temperature-sensitive substrates such as PET.

AUTHOR CONTRIBUTIONS

Martin Rudolph: Conceptualization, writing original draft, formal analysis, investigation, writing review and editing. **Peter Birtel**: Investigation, writing review and editing. **Thomas Arnold**: Writing review and editing,

16128869, 0, Downloaded from https://onlinelibrary.wiley.com/doi/10.1002/ppap.202200229 by Cochrane Germany, Wiley Online Library on [21/03/2023]. See the Terms and Conditions (https://onlinelibrary.wiley.com/terms-and-conditions) on Wiley Online Library for rules of use; OA articles are governed by the applicable Creative Commons License

resources. **Andrea Prager**: Investigation. **Sergej Naumov**: Methodology. **Ulrike Helmstedt**: Writing review and editing. **André Anders**: Writing review and editing, funding. **Patrick C. With**: Conceptualization, investigation, formal analysis, writing original draft, writing review and editing.

ACKNOWLEDGMENTS

This work was partially funded by the Free State of Saxony and the European Regional Development Fund (Grant No. 100336119).

DATA AVAILABILITY STATEMENT

The data that support the findings of this study are available from the corresponding author upon reasonable request.

ORCID

Martin Rudolph http://orcid.org/0000-0002-0854-6708
Peter Birtel http://orcid.org/0000-0003-4840-0428
Thomas Arnold http://orcid.org/0000-0002-3666-2415
Andrea Prager http://orcid.org/0000-0002-3981-9019
Ulrike Helmstedt http://orcid.org/0000-0003-2345-3742
André Anders http://orcid.org/0000-0002-5313-6505
Patrick C. With http://orcid.org/0000-0002-9461-8877

REFERENCES

[1] B. Twomey, D. Dowling, G. Byrne, L. O'Neill, L.-A. O'Hare, *Plasma Processes Polym.* **2007**, *4*, S450. https://doi.org/10.1002/ppap.200731205

[2] J. S. Lewis, M. S. Weaver, *IEEE J. Sel. Top. Quantum Electron.* **2004**, *10*, 45. https://doi.org/10.1109/jstqe.2004.824072

[3] S. Castro-Hermosa, M. Top, J. Dagar, J. Fahlteich, T. M. Brown, *Adv. Electron. Mater.* **2019**, *5*, 1800978. https://doi.org/10.1002/aelm.201800978

[4] A. Uddin, M. Upama, H. Yi, L. Duan, *Coatings* **2019**, *9*, 65. https://doi.org/10.3390/coatings9020065

[5] K. Inomata, H. Ha, K. A. Chaudhary, H. Koinuma, *Appl. Phys. Lett.* **1994**, *64*, 46. https://doi.org/10.1063/1.110916

[6] L. J. Ward, W. C. E. Schofield, J. P. S. Badyal, A. J. Goodwin, P. J. Merlin, *Langmuir* **2003**, *19*, 2110. https://doi.org/10.1021/la0204287

[7] S. E. Babayan, J. Y. Jeong, A. Schütze, V. J. Tu, M. Moravej, G. S. Selwyn, R. F. Hicks, *Plasma Sources Sci. Technol.* **2001**, *10*, 573. https://doi.org/10.1088/0963-0252/10/4/305

[8] J. Chen, J. H. Davidson, *Plasma Chem. Plasma Process.* **2004**, *24*, 169. https://doi.org/10.1023/B:PCPP.0000013197.77036.f5

[9] J. Salge, *Surf. Coat. Technol.* **1996**, *80*, 1. https://doi.org/10.1016/0257-8972(95)02676-2

[10] A. Sonnenfeld, T. M. Tun, L. Zajíčková, K. V. Kozlov, H. E. Wagner, J. F. Behnke, R. Hippler, *Plasmas Polym.* **2001**, *6*, 237. https://doi.org/10.1023/a:1014414016164

[11] G. R. Nowling, S. E. Babayan, V. Jankovic, R. F. Hicks, *Plasma Sources Sci. Technol.* **2002**, *11*, 97. https://doi.org/10.1088/0963-0252/11/1/312

[12] M. Moravej, R. F. Hicks, *Chem. Vap. Deposition* **2005**, *11*, 469. https://doi.org/10.1002/cvde.200400022

[13] Y. Sawada, S. Ogawa, M. Kogoma, *J. Phys. D: Appl. Phys.* **1995**, *28*, 1661. https://doi.org/10.1088/0022-3727/28/8/015

[14] K. Schmidt-Szalowski, Z. Rżanek-Boroch, J. Sentek, Z. Rymuza, Z. Kusznierewicz, M. Misiak, *Plasmas Polym.* **2000**, *5*, 173. https://doi.org/10.1023/a:1011314420080

[15] L. O'Neill, L. A. O'Hare, S. R. Leadley, A. J. Goodwin, *Chem. Vap. Deposition* **2005**, *11*, 477. https://doi.org/10.1002/cvde.200404209

[16] A. P. Roberts, B. M. Henry, A. P. Sutton, C. R. M. Grovenor, G. A. D. Briggs, T. Miyamoto, M. Kano, Y. Tsukahara, M. Yanaka, *J. Membr. Sci.* **2002**, *208*, 75. https://doi.org/10.1016/s0376-7388(02)00178-3

[17] J.-H. Tsai, S.-M. Hsu, I. C. Cheng, C.-C. Hsu, J.-Z. Chen, *Ceram. Int.* **2019**, *45*, 22078. https://doi.org/10.1016/j.ceramint.2019.07.224

[18] E. Mudra, M. Streckova, D. Pavlinak, V. Medvecka, D. Kovacik, A. Kovalcikova, P. Zubko, V. Girman, Z. Dankova, V. Koval, J. Duzsa, *Appl. Surf. Sci.* **2017**, *415*, 90. https://doi.org/10.1016/j.apsusc.2016.11.162

[19] M. Černák, L. Černáková, I. Hudec, D. Kováčik, A. Zahoranová, *Eur. Phys. J.: Appl. Phys.* **2009**, *47*, 22806. https://doi.org/10.1051/epjap/2009131

[20] V. Medvecká, D. Kováčik, A. Zahoranová, M. Černák, *Appl. Surf. Sci.* **2018**, *428*, 609. https://doi.org/10.1016/j.apsusc.2017.09.178

[21] J. V. Alemán, A. V. Chadwick, J. He, M. Hess, K. Horie, R. G. Jones, P. Kratochvíl, I. Meisel, I. Mita, G. Moad, S. Penczek, R. F. T. Stepto, *Pure Appl. Chem.* **2007**, *79*, 1801. https://doi.org/10.1351/pac200779101801

[22] Y. Zhao, D. G. Truhlar, *Acc. Chem. Res.* **2008**, *41*, 157. https://doi.org/10.1021/ar700111a

[23] N. Beyer, G. Steinfeld, V. Lozan, S. Naumov, R. Flyunt, B. Abel, B. Kersting, *Chem. - Eur. J.* **2017**, *23*, 2303. https://doi.org/10.1002/chem.201604460

[24] F. Stolz, J. Appun, S. Naumov, C. Schneider, B. Abel, *ChemPlusChem* **2017**, *82*, 233. https://doi.org/10.1002/cplu.201600347

[25] P. C. With, J. Lehnert, L. Seifert, S. Dietrich, H. Krautscheid, S. Naumov, A. Prager, B. Abel, L. Prager, U. Helmstedt, *Appl. Surf. Sci.* **2019**, *493*, 525. https://doi.org/10.1016/j.apsusc.2019.06.272

[26] I. Schrödinger, *Jaguar, version 8.5* **2014**.

[27] P. J. Hay, W. R. Wadt, *J. Chem. Phys.* **1985**, *82*, 299. https://doi.org/10.1063/1.448975

[28] L. Prager, A. Dierdorf, H. Liebe, S. Naumov, S. Stojanović, R. Heller, L. Wennrich, M. R. Buchmeiser, *Chem. - Eur. J.* **2007**, *13*, 8522. https://doi.org/10.1002/chem.200700351

[29] Y. Berdichevsky, J. Khandurina, A. Guttman, Y. H. Lo, *Sens. Actuators, B* **2004**, *97*, 402. https://doi.org/10.1016/j.snb.2003.09.022

[30] L. Prager, U. Helmstedt, H. Herrnberger, O. Kahle, F. Kita, M. Münch, A. Pender, A. Prager, J. W. Gerlach, M. Stasiak, *Thin Solid Films* **2014**, *570*, 87. https://doi.org/10.1016/j.tsf.2014.09.014

[31] R. Foest, E. Kindel, H. Lange, A. Ohl, M. Stieber, K. D. Weltmann, *Contrib, Plasma Phys.* **2007**, *47*, 119. https://doi.org/10.1002/ctpp.200710017

[32] A. F. Ismail, K. C. Khulbe, T. Matsuura, *Gas Separation Membranes*, Springer, Cham **2015**.

16128869, 0, Downloaded from https://onlinelibrary.wiley.com/doi/10.1002/ppap.202200229 by Cochrane Germany, Wiley Online Library on [21/03/2023]. See the Terms and Conditions (https://onlinelibrary.wiley.com/terms-and-conditions) on Wiley Online Library for rules of use; OA articles are governed by the applicable Creative Commons License

[33] D. W. Breck, *Chemistry and Use*, John Wiley & Sons, New York, London, Sydney, and Toronto **1974**.

SUPPORTING INFORMATION

Additional supporting information can be found online in the Supporting Information section at the end of this article.

How to cite this article: M. Rudolph, P. Birtel, T. Arnold, A. Prager, S. Naumov, U. Helmstedt, A. Anders, P. C. With, *Plasma. Process. Polym.* **2023**, e2200229. https://doi.org/10.1002/ppap.202200229

16128869, 0, Downloaded from https://onlinelibrary.wiley.com/doi/10.1002/ppap.202200229 by Cochrane Germany, Wiley Online Library on [21/03/2023]. See the Terms and Conditions (https://onlinelibrary.wiley.com/terms-and-conditions) on Wiley Online Library for rules of use; OA articles are governed by the applicable Creative Commons License